Higgs and $Z \to \tau^+\tau^-$ in CMS

Christian Veelken
Department of Physics, University of California, Davis, USA

The production of oppositely–charged tau lepton pairs is studied at 7 TeV center–of–mass energy using 36 pb^{-1} of proton-proton collision data collected by the CMS experiment in 2010. Events are selected in a combination of different final states resulting from hadronic and leptonic tau decays. The $Z \to \tau^+\tau^-$ cross–section is measured. The tau–pair kinematics is fully reconstructed using a likelihood technique. The mass spectrum observed in data is used to derive upper bounds on the production cross section times branching ratio to tau–pairs as a function of the Higgs boson mass in the Minimal Supersymmetric extension of the Standard Model (MSSM).

1 Introduction

We report on the results of an analysis of oppositely charged tau lepton pairs, produced in pp collisions at $\sqrt{s} = 7$ TeV at the Large Hadron Collider (LHC). The analyzed dataset corresponds to an integrated luminosity of 36 pb^{-1} and has been recorded by the Compact Muon Solenoid (CMS) experiment in 2010.

Within the Standard Model (SM), the process $pp \to Z + X$, $Z \to \tau^+\tau^-$ constitutes the dominant source of tau lepton pairs considered in our study. $Z \to \tau^+\tau^-$ events are useful for measuring tau identification and trigger efficiencies. On the other hand, $Z \to \tau^+\tau^-$ events constitute an important irreducible background in searches for new physics. We measure the $Z \to \tau^+\tau^-$ production cross–section in a combination of four decay modes: $\tau^+\tau^- \to e\mu$, $\mu\mu$, $e\tau_{had}$ and $\mu\tau_{had}$, where we denote by τ_{had} a reconstructed hadronic decay of a tau.

We search for evidence for MSSM neutral Higgs bosons in the tau–pair mass spectrum observed in data. The tau lepton pair mass is reconstructed by a novel likelihood based algorithm.

2 CMS detector and coordinate system

The CMS detector is described in detail in[1].

CMS uses a right–handed coordinate system, with the origin at the nominal interaction point, the x axis pointing to the centre of the LHC, the y axis pointing up perpendicular to the LHC plane, and the z axis along the counterclockwise–beam direction. The polar angle θ is measured from the positive z axis and the azimuthal angle ϕ is measured in the xy plane. We will refer to the direction of particles also in terms of the pseudo–rapidity $\eta = -\ln\left(\tan\frac{\theta}{2}\right)$ and denote by p_T the component of particle momentum transverse to the beam direction.

3 Lepton reconstruction and identification

Electrons are reconstructed by combining energy deposits in the electromagnetic calorimeter with tracks in the silicon pixel and strip detectors[2]. Selection criteria are applied[3] to reduce the rates with which charged hadrons and neutral pions/photons are identified as electrons.

Muons are reconstructed in the tracking detectors and in dedicated muon chambers[4]. Quality cuts are applied[3] to ensure that muons are well reconstructed.

Electrons and muons are required to be isolated in the detector[5], in order to remove leptons originating from hadron decays, which are typically found within jets.

Tau lepton hadronic decays are reconstructed and identified by the Hadron plus Strips (HPS) algorithm[6]. The algorithm uses as input collections of particles reconstructed by the CMS particle flow (PF) algorithm[7,8]. π^0 meson candidates are build by clustering electrons and photons reconstructed by the PF algorithm in "strips" along the bending plane of the 4 T CMS magnetic field, taking into account the possible broadening of calorimeter signatures by photon conversions within the tracking detectors. From the list of charged hadrons plus π^0 candidates, different τ_{had} decay hypotheses are build, corresponding to specific hadronic tau decay modes. The HPS algorithm considers all possible combinations of charged hadrons and π^0 candidates and selects combinations which are consistent with specific hadronic tau decay modes. In case multiple hypotheses are consistent, the algorithm chooses the combination which is most isolated in terms of the presence of nearby reconstructed particles. Requirements on isolation variables define different working–points in the space of tau identification efficiency vs. jet–to–tau misidentification rate. We require that other than the τ_{had} constituents there be no charged hadrons of $p_T > 1.0$ GeV and no π^0 candidates of $p_T > 1.5$ GeV within a cone of size $\Delta R = 0.5$ around the tau direction.

Jets are build using the anti–k_T algorithm[9] from particles reconstructed by the PF algorithm not identified as electrons, muons or hadronic tau decays. Jet energy corrections are applied[10].

The missing transverse energy E_T^{miss} is measured using the collection of particles reconstructed by the PF algorithm.

4 Event selection

Events selected in the $e\mu$, $\mu\mu$ and $\mu\tau_{had}$ decay channels are triggered by single muon triggers. P_T thresholds of the muon triggers vary between 9–15 GeV, depending on instantaneous luminosity. $e\tau_{had}$ events are triggered by a combination of single electron triggers with P_T thresholds 8–12 GeV plus a dedicated $e\tau_{had}$ trigger. The $e\tau_{had}$ trigger runs a simplified version of the offline tau reconstruction algorithm with less stringent selection criteria and rejects events without hadronic tau decays. The requirement of a loosely identified τ_{had} reduces the trigger rate considerably and allows to keep the electron P_T threshold of the $e\tau_{had}$ trigger at 12 GeV.

The offline selection of $e\tau_{had}$ and $\mu\tau_{had}$ events requires the presence of an isolated electron or muon with $p_T > 15$ GeV and $|\eta| < 2.1$ and a τ_{had} of opposite charge with $p_T > 20$ GeV, $|\eta| < 2.3$. The transverse mass $M_T(\ell, E_T^{\text{miss}}) = \sqrt{2p_T^{\ell} E_T^{\text{miss}} (1 - \cos\Delta\phi)}$, where $\Delta\phi$ is the difference in azimuth between the E_T^{miss} vector and either e or μ, is required to be below 40 GeV, in order to reduce W + jets background. Events with two isolated electrons or muons are rejected in order to remove Drell–Yan background.

Events in the $e\mu$ channel are selected by requiring an isolated muon within $|\eta| < 2.1$, plus an oppositely charged electron within $|\eta| < 2.4$, both with $p_T > 15$ GeV. W + jet and $t\bar{t}$ backgrounds are removed by requiring $M_T(e, E_T^{\text{miss}}) < 50$ GeV and $M_T(\mu, E_T^{\text{miss}}) < 50$ GeV.

Events in the $\mu\mu$ channel are required to have two muons of opposite charge with $|\eta| < 2.1$. The transverse momentum of the higher (lower) p_T muon is required to exceed 19 GeV (10 GeV). We further require $\Delta\phi_{\mu\mu} < 2.0$ for the azimuthal angle between the two muons, to remove QCD

background events in which muons result from quarkonia decays or from decay chains of heavy–flavored hadrons. W + jet and $t\bar{t}$ backgrounds are removed by requiring $E_T^{\rm miss} < 50$ GeV. Drell–Yan dimuon background is removed by a multivariate likelihood technique[5].

5 Background estimation

The main backgrounds are QCD multi–jet, W + jet and Drell–Yan events. Small additional background contributions are due to $t\bar{t}$ and diboson (WW, WZ, ZZ) events. Background contributions are estimated from data.

Two complementary data–driven methods are used to estimate background contributions in the $e\tau_{had}$ and $\mu\tau_{had}$ channels: The first method is based on the charge of μ plus τ_{had} and the extrapolation of background contributions measured in a high M_T sideband. The QCD background is estimated by measuring the ratio of same–sign (SS) to opposite–sign (OS) events in a control region defined by inverting the isolation criteria for electrons and muons. The measured OS/SS ratio is used to extrapolate the QCD event yield measured in another control region, identical to the signal region except that e and τ_{had} (μ and τ_{had}) are required to be of the same charge, into the signal region. A correction is applied to account for W + jet and other backgrounds, for which the OS/SS ratio may be different. The contribution of W + jet background in the control region and in the signal region is estimated by extrapolating the event yields measured in $M_T(\ell, E_T^{\rm miss}) > 60$ GeV sidebands into $M_T(\ell, E_T^{\rm miss}) < 40$ GeV regions. The second method is based on measuring jet–to–tau misidentification rates in event samples dominated by QCD and W + jet backgrounds, relaxing the τ_{had} identification criteria in the $Z \to \tau^+\tau^-$ event selection and applying the measured misidentification rates as weights to events which pass all event selection requirements except τ_{had} identification criteria.

In the $\mu\mu$ channel the dominant Drell–Yan background is estimated by selecting events with a reduced likelihood from which one of the input variables is excluded and fitting with signal and background templates the distribution of the excluded variable obtained after cutting on the reduced likelihood and applying all other event selection requirements. Contributions of other backgrounds to the $\mu\mu$ channel as well as background contributions to the $e\mu$ channel are small. Further details of estimating background contributions can be found in[5].

	$e\mu$	$\mu\mu$ ($M_{\mu\mu} < 70$ GeV)	$e\tau_{had}$	$\mu\tau_{had}$
$Z \to \ell^+\ell^-$, jet misidentified as τ	-		15.0 ± 6.2	6.4 ± 2.4
$Z \to \ell^+\ell^-$, lepton misidentified as τ	2.4 ± 0.3	20.1 ± 1.3	109 ± 28	12.9 ± 3.5
$t\bar{t}$	7.1 ± 1.3	0.15 ± 0.03	2.6 ± 1.3	6.0 ± 3.0
$W \to \ell\nu$	1.5 ± 0.5	2.5 ± 2.5	30.6 ± 3.1	54.9 ± 4.8
$W \to \tau\nu$			7.0 ± 0.7	14.7 ± 1.3
QCD multi–jet			181 ± 23	132 ± 14
$WW/WZ/ZZ$	3.0 ± 0.4	-	0.8 ± 0.4	1.6 ± 0.8
Total background	14.0 ± 1.8	22.8 ± 2.8	346 ± 37	228 ± 16
Total data	101	58	540	517

Table 1: Number of events expected in the $e\mu$, $\mu\mu$, $e\tau_{had}$ and $\mu\tau_{had}$ decay channels from different background processes. The uncertainties quoted in the table represent combined statistical plus systematic uncertainties on the background estimates. The number of events observed in each decay channel is given in the bottom row.

The background estimates obtained for all four channels are given in Tab. 1. The number of events expected in each decay channel is compared to the number of events observed in data. The difference between the number of events observed in data and the expected background total represents the signal.

6 Systematic uncertainties

Electron and muon reconstruction, identification, isolation and trigger efficiencies are measured in data, using the "tag–and–probe" method[3]. The resulting uncertainty on the signal efficiency varies between less than 1% and 3%, depending on decay channel.

In the $e\tau_{had}$ and $\mu\tau_{had}$ decay channels the by far dominant systematic uncertainty in the efficiency with which hadronic tau decays are reconstructed and identified. The τ_{had} efficiency is measured in data. At present the measurement is statistically limited and has an uncertainty of 23%.

The effect of energy scale uncertainties on the signal efficiency as well as on the shape of mass spectra is estimated by varying the energy and momentum of reconstructed objects within their respective uncertainties, recomputing all kinematic quantities and repeating the event selection. The energy scale uncertainty amounts to 2% for electrons, 1% for muons and 3% for τ_{had} decays. The uncertainty on the energy of jets with $p_T > 10$ GeV amounts to 3%. The energy of particles neither identified as e, μ or τ_{had} nor contained within a jet of $p_T > 10$ GeV is varied by 10%.

7 $Z \to \tau^+\tau^-$ cross–section measurement

The Z production cross–section times branching ratio for the decay into tau–pairs is extracted via the relation:

$$\sigma\left(pp \to Z + X\right) \times BR\left(Z \to \tau^+\tau^-\right) = \frac{N}{A \cdot \varepsilon \cdot B' \cdot L}.$$

N denotes the number of signal events, B' the branching fraction of the decay mode considered[11], and L the integrated luminosity of the analyzed dataset. The signal acceptance A represents the probability of the visible tau decay products to pass p_T and η cuts. The efficiency for signal events to pass all other event selection criteria is denoted by ε.

The number of signal events is determined by fitting the $e\mu$, $\mu\mu$, $e\tau_{had}$ and $\mu\tau_{had}$ visible mass distributions observed in data by shape templates for signal and background processes. Shape templates for QCD and Drell–Yan backgrounds are obtained from data. Templates for other background processes and for the $Z \to \tau^+\tau^-$ signal are taken from the Monte Carlo simulation[a]. All shape templates taken from the simulation are parametrized as function of e, μ and τ_{had} energy scales. The energy scales are allowed to vary during the fit, within their uncertainties. The background estimates obtained from data and shown in Tab. 1 enter the fit as constraints, with uncertainties given in the table.

The results of the fits are illustrated in Fig. 1, which compares the visible mass distributions observed in data to the sum of signal and background templates scaled by the yields obtained by the four individual fits. Good agreement is observed in all channels.

Final state	$\sigma\left(pp \to Z + X\right) \times BR\left(Z \to \tau^+\tau^-\right)$	stat.	syst.	lumi.	τ_{had}–ID eff.
$e\mu$	0.99	0.12	0.06	0.04	-
$\mu\mu$	1.14	0.27	0.04	0.05	-
$e\tau_{had}$	0.94	0.11	0.03	0.04	0.22
$\mu\tau_{had}$	0.83	0.07	0.04	0.03	0.19

Table 2: Z production cross–section times branching fraction for decay $Z \to \tau^+\tau^-$, measured in the four decay channels $e\mu$, $\mu\mu$, $e\tau_{had}$ and $\mu\tau_{had}$. The uncertainty associated to the efficiency to reconstruct and identified τ_{had} decays is shown separately from other systematic uncertainties. All numbers given in the table are in units of nb.

[a] It has been verified in background dominated control regions that the visible mass distributions for background processes are well modeled by the Monte Carlo simulation.

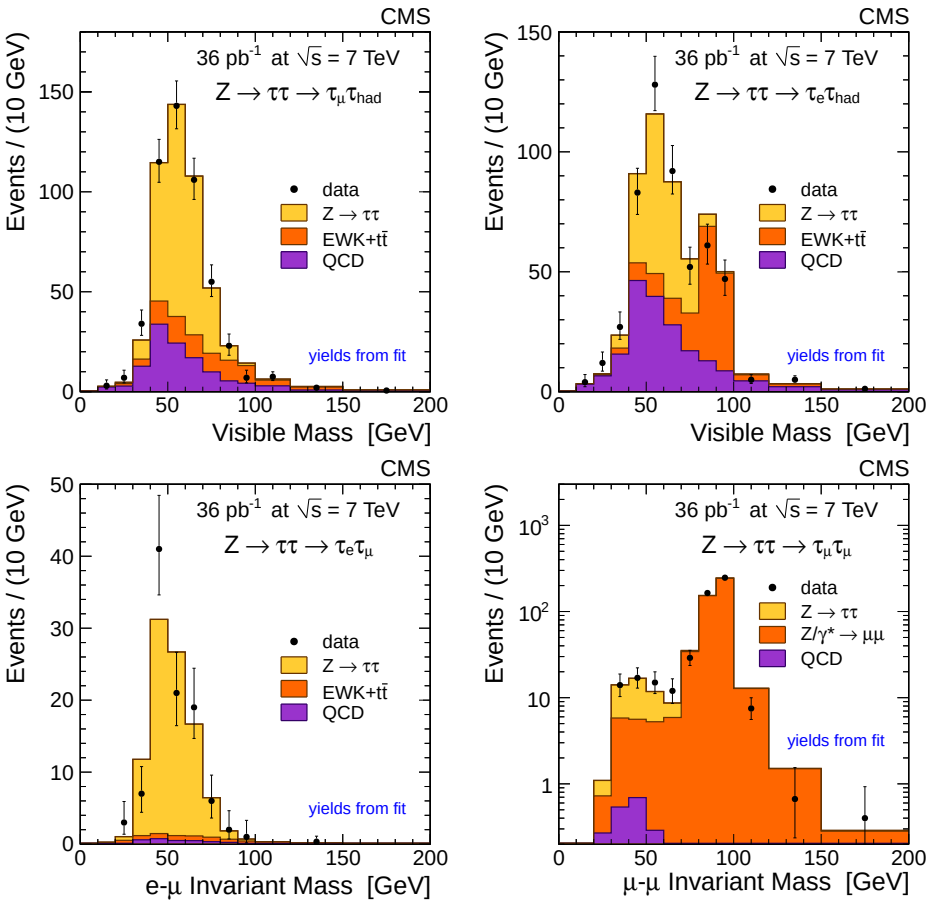

Figure 1: Visible mass spectra observed in data compared to shape templates of signal and background processes scaled by the yields obtained by fits of individual decay channels.

The $\sigma\,(pp \to Z + X) \times BR\,(Z \to \tau^+\tau^-)$ cross–section values extracted from the fits are given in Tab. 2. The cross–sections are quoted for $Z \to \tau^+\tau^-$ production within the mass window $60 < M_{\tau^+\tau^-} < 120$ GeV. Contributions from $Z/\gamma^* \to \tau^+\tau^-$ events outside the mass window are small (between $1-3\%$, depending on decay channel) and accounted for by correction factors.

Measured cross–sections are compatible with each other and in good agreement with the NNLO theoretical prediction[12] 0.972 ± 0.042 nb. The measured $Z \to \tau^+\tau^-$ cross–sections also agree well with the corresponding CMS measurement in $Z \to e^+e^-$ and $Z \to \mu^+\mu^-$ events[3]:

$$\sigma\,(pp \to Z + X) \times BR\left(Z \to e^+e^-, \mu^+\mu^-\right) = 0.931 \pm 0.026\ (\text{stat.}) \pm 0.023\ (\text{sys.}) \pm 0.102\ (\text{lumi.})\ \text{nb}.$$

In the $e\tau_{had}$ and $\mu\tau_{had}$ channels the precision of the cross–section measurement is limited by the uncertainty on the τ_{had} identification efficiency. A simultaneous fit of all four channels is performed in order to obtain $\sigma\,(pp \to Z + X) \times BR\,(Z \to \tau^+\tau^-)$ together with a scale–factor which represents the ratio of τ_{had}–ID efficiency in data to simulation. The result of the simultaneous fit is illustrated in Fig. 2 (left), showing the likelihood contours in the plane of cross–section versus scale–factor. The cross–section extracted from the simultaneous fit is:

$$\sigma\,(pp \to Z + X) \times BR\left(Z \to \tau^+\tau^-\right) = 1.00 \pm 0.05\ (\text{stat.}) \pm 0.08\ (\text{sys.}) \pm 0.04\ (\text{lumi.})\ \text{nb}.$$

The value of $\sigma\,(pp \to Z + X) \times BR\,(Z \to \tau^+\tau^-)$ obtained from the simultaneous fit is compared to the cross–sections measured individually for the four decay channels in Fig. 2 (right). The value of the τ_{had}–ID efficiency scale–factor obtained from the simultaneous fit is 0.93 ± 0.09.

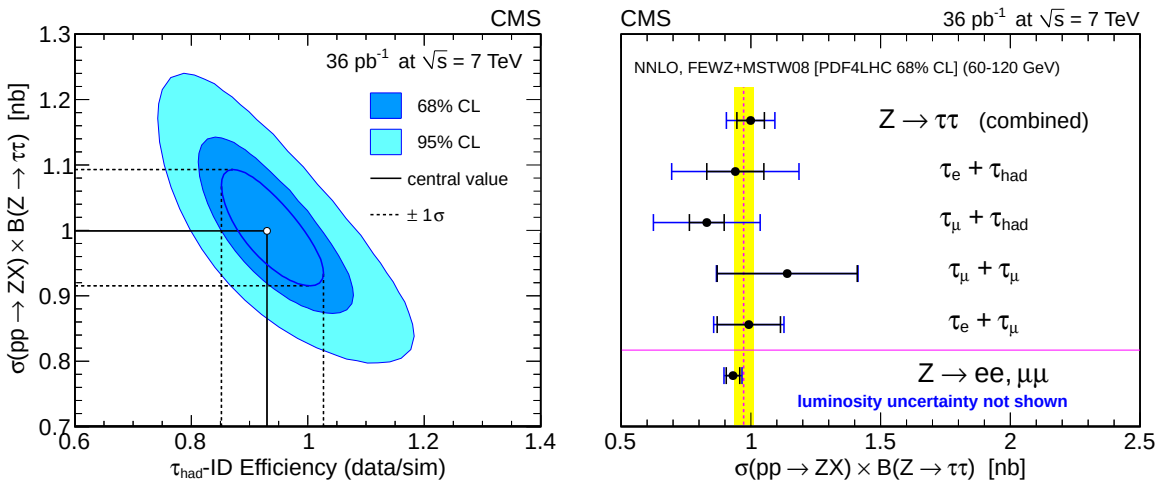

Figure 2: Left: Likelihood contours for the simultaneous fit of $e\mu$, $\mu\mu$, $e\tau_{had}$ and $\mu\tau_{had}$ decay channels. The inner (outer) ellipse indicates the region of 68% (95%) coverage in the $\sigma\left(pp \to Z + X\right) \times BR\left(Z \to \tau^{+}\tau^{-}\right)$ versus τ_{had}–ID efficiency scale–factor plane. The dashed lines indicate the one standard–deviation uncertainties on either one of the two parameters, obtained by marginalization of the second parameter. Right: Graphical representation of the cross–sections measured in individual decay channels compared to the result of the simultaneous fit. The shaded band represents the NNLO theoretical prediction and its uncertainty.

A more precise determination of the τ_{had}–ID efficiency is possible by relating the cross–section measured in the $Z \to \tau^{+}\tau^{-}$ channel to the cross–sections measured by CMS in the $Z \to e^{+}e^{-}$ and $Z \to \mu^{+}\mu^{-}$ channels, as systematic uncertainties partially cancel. The τ_{had}–ID efficiency obtained via this method is 0.96 ± 0.07 .

8 Search for neutral MSSM Higgs bosons

We search for evidence for neutral Higgs bosons in the tau–pair mass spectra observed in data. The results are interpreted in the minimal supersymmetric extension to the standard model (MSSM). In this model two Higgs doublets yield five massive Higgs bosons: a light neutral scalar (h), two charged scalars ($H^{\pm}$), a heavy neutral scalar (H) and a pseudo–scalar (A).

The Higgs boson signal is distinguished from backgrounds via the "full" mass, denoted by $M_{\tau^{+}\tau^{-}}$, of the tau–pair, reconstructed by a novel likelihood technique. The likelihood is build from three terms: the tau decay phase–space, the probability density in the tau transverse momentum, parametrized as a function of the tau pair mass, and the compatibility of the sum of neutrino momenta with the measured value of $E_T^{\rm miss}$. The product of the three terms is maximized with respect to the free parameters in the likelihood functions: the energies and directions of the neutrinos produced in the tau decays. The momenta of visible tau decay products are fixed to their measured values. The algorithm yields a tau pair mass solution for each event, with mean consistent with the true value and nearly Gaussian resolution. For a Higgs of mass 130 GeV a resolution of $\sim 21\%$ is attained. The data is in agreement with the expectation for background processes. No evidence for a Higgs signal is seen.

In the absence of evidence for a Higgs signal, we set limits on the product of Higgs boson production cross–section times branching fraction for the decay into tau pairs, which we denote by $\sigma_{\Phi}\cdot B_{\tau\tau}$. The limit is computed as function of m_A by fitting the $M_{\tau^{+}\tau^{-}}$ distribution observed in the $e\mu$, $e\tau_{had}$ and $\mu\tau_{had}$ decay channels with shape templates for different Higgs mass hypotheses, obtained from Monte Carlo simulation. We use a Bayesian approach with a uniform prior on $\sigma_{\Phi}\cdot B_{\tau\tau}$ to set the limit. Systematic uncertainties on fit parameters corresponding to background normalization, signal efficiencies and energy scales are represented by nuisance parameters and

removed by marginalization, assuming a log–normal prior for normalization parameters and signal efficiencies and Gaussian priors for energy scale parameters. The effect of energy scale parameters on the shape of $M_{\tau^+\tau^-}$ mass templates is modeled via a continuous alteration of the shape[13].

For a given mass hypothesis m_A the product of signal acceptance times efficiency is computed by weighting acceptances and efficiencies for h, H and A bosons according to cross–section. Higgs cross–sections entering the weighting procedure are computed for $\tan\beta = 30$. Acceptance times efficiency values are averaged over the two production processes $gg \to \Phi$ (gluon fusion through a b quark loop) and $b\bar{b} \to \Phi$ (direct $b\bar{b}$ annihilation from the b parton density in the beam protons). Differences between scalar and pseudo–scalar Higgs bosons and between the $gg \to \Phi$ and $b\bar{b} \to \Phi$ production mechanisms ($\lesssim 10\%$) are taken into account as systematic uncertainty.

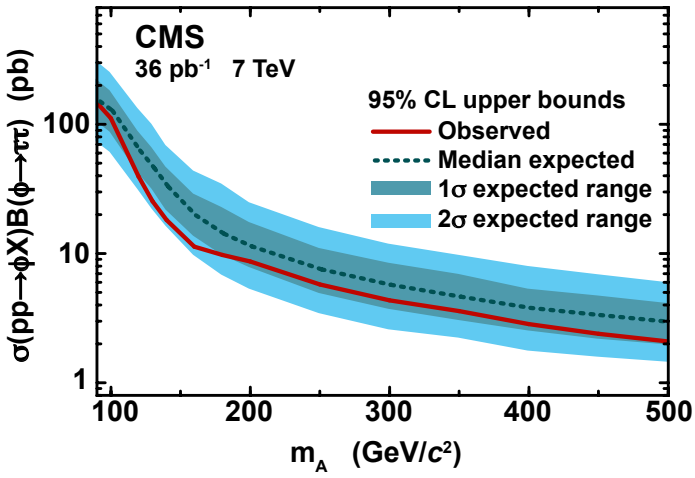

Figure 3: Observed 95% confidence level (CL) upper limit on $\sigma_\Phi \cdot B_{\tau\tau}$. The (dark) light shaded band indicates the one (two) standard–deviation range of experimental outcomes expected for background–only experiments, given the sensitivity of our analysis and 36 pb^{-1} of data.

The resulting limit on $\sigma_\Phi \cdot B_{\tau\tau}$ is shown in Fig. 3 (see[14] for tabulated values). The observed limit is within the range of experimental outcomes expected for background–only experiments.

We interpret the limit on $\sigma_\Phi \cdot B_{\tau\tau}$ in the m_h^{max} scenario of the MSSM and convert it into a corresponding limit on the MSSM parameters $\tan\beta$ versus m_A. Higgs boson cross–section values reported by the LHC Higgs Cross–section Working Group[15] are used for the conversion. For the $b\bar{b} \to \Phi$ cross–section we take the values computed in the 5–flavor scheme. The limits obtained on $\tan\beta$ versus m_A are shown in Fig. 4.

Our results exclude a region in $\tan\beta$ down to values smaller than those excluded by TeVatron experiments[16] for $m_A \lesssim 140$ GeV. For larger m_A our results significantly extend the previously excluded region. The region in $\tan\beta$ versus m_A parameter space excluded by LEP experiments[17] is also shown in the figure.

9 Summary

Tau lepton pair production has been analyzed in 36 pb^{-1} of pp collision data recorded by the CMS experiment in 2010. The measured Z production cross–section times branching fraction for the decay into tau pairs,

$\sigma\,(pp \to Z + X) \times BR\,(Z \to \tau^+\tau^-) = 1.00 \pm 0.05\ (\text{stat.}) \pm 0.08\ (\text{sys.}) \pm 0.04\ (\text{lumi.})$ nb,

is in agreement with NNLO theoretical predictions and with CMS measurements of the Z production cross–section in the $Z \to e^+e^-$ and $Z \to \mu^+\mu^-$ channels. The observed $Z \to \tau^+\tau^-$

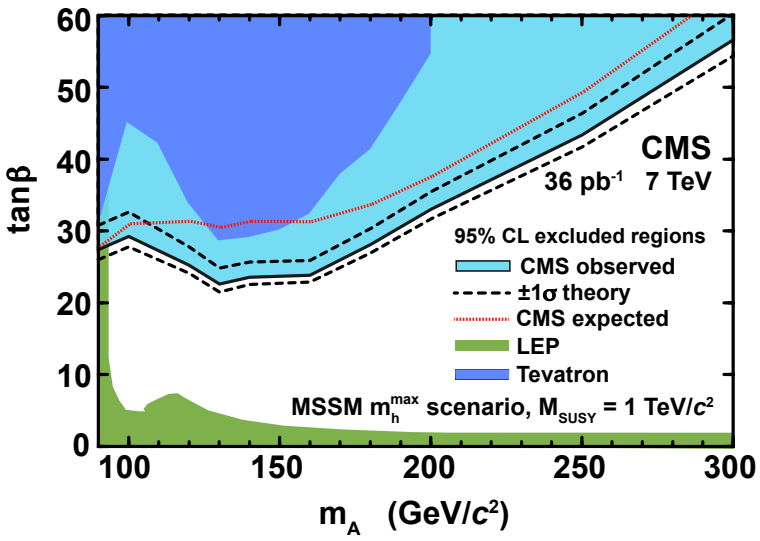

Figure 4: Region in $\tan\beta$ versus m_A parameter space excluded by CMS data at 95% CL. Theoretical uncertainties are represented by black dashed lines, enclosing the observed limit. Limits obtained by previous experiments at TeVatron and at LEP are indicated separately by shaded regions.

yield allows to determine the hadronic tau identification efficiency with an uncertainty of 7%.

No evidence for neutral MSSM Higgs boson production is observed in the distribution of the "full" tau lepton pair mass, reconstructed by a novel likelihood technique. A limit on Higgs boson cross-section times branching fraction for the decay into tau pairs is set. The observed limit excludes a significant region in the MSSM $\tan\beta$ versus m_A parameter space not previously explored by experiments at the TeVatron and at LEP.

References

1. R. Adolphi *et al*, *JINST* **0803**, S08004 (2008).
2. CMS Collaboration, CMS–PAS–EGM–10–004, http://cdsweb.cern.ch/record/1299116.
3. CMS Collaboration, *JHEP* **01**, 080 (2011).
4. CMS Collaboration, CMS–PAS–MUO–10–002, http://cdsweb.cern.ch/record/1279140.
5. CMS Collaboration, arXiv:1104.1617 [hep–ex], submitted to *JHEP.*
6. *CMS Collaboration, CMS–PAS–TAU–11–001, http://cdsweb.cern.ch/record/1337004.*
7. *CMS Collaboration, CMS–PAS–PFT–09–001, http://cdsweb.cern.ch/record/1194487.*
8. *CMS Collaboration, CMS–PAS–PFT–10–002, http://cdsweb.cern.ch/record/1279341.*
9. *M. Cacciari, G. P. Salam and G. Soyez,* JHEP **0804**, *063 (2008).*
10. *CMS Collaboration, CMS–PAS–JME–10–010, http://cdsweb.cern.ch/record/1308178.*
11. *K. Nakamura et al,* J. Phys. *G* **37**, *075021 (2010).*
12. *K. Melnikov and F. Petriello,* Phys. Rev. *D* **74**, *114017 (2006).*
13. *J. S. Conway, arXiv:1103.0354 [hep–ex], submitted to Proceedings of PhyStat 2011.*
14. *CMS Collaboration, arXiv:1104.1619 [hep–ex].*
15. *S. Dittmaier et al, arXiv:1101.0593 [hep–ph].*
16. *Tevatron New Physics and Higgs Working Group, arXiv:1003.3363 [hep–ex].*
17. *LEP Higgs Working Group, EPJC* **47**, *547 (2006).*